PROPAGATION THROUGH ELECTRICALLY COUPLED CELLS

Effects of a Resistive Barrier

RONALD W. JOYNER, RICHARD VEENSTRA, DAVID RAWLING, AND ALFREDO CHORRO
Department of Physiology and Biophysics, University of Iowa, Iowa City, Iowa 52242

ABSTRACT Action potential propagation through cardiac tissue occurs in a spatially inhomogeneous three-dimensional electrical syncytium composed of discrete cells with regional variations in membrane properties and intercellular resistance. In comparison with axons, cardiac tissue presents some differences in the application of core conductor cable theory. We have used analytical and numerical techniques to contrast the propagation of action potentials along nerve axons and along cardiac strands, including an explicit inclusion of cellular anatomical factors (the surface-to-volume ratio), the strand radius, and the regional distribution of longitudinal resistance. A localized decrease in the number of gap junctions will produce a functional resistive barrier, which can lead to unidirectional block of propagation if the tissue on two sides of the barrier differ in either excitability or passive electrical load. However, in some circumstances, a resistive barrier separating regions of different electrical load can actually facilitate propagation into the region of larger electrical load.

INTRODUCTION

Action potential propagation through cardiac tissue occurs from cell to cell through a three-dimensional electrical syncytium. There are obvious analogies between a cardiac strand and a continuous nerve axon that have been used to model cardiac action potential propagation (Lieberman et al., 1973; Sharp and Joyner, 1980). More recently, the discrete nature of the cardiac syncytium has been shown both experimentally (Spach et al., 1981) and theoretically (Joyner, 1982) to produce changes in action potential shape and conduction velocity, which are not predicted by continuous propagation models. Spach et al. (1982) refer to the discontinuities as microscopic (when the syncytium is relatively isolated into single cells or small groups of cells by a relative lack of cell-cell couplings) or macroscopic (reflecting the anatomical features of branching trabeculae, regions of decreased cell-cell coupling, etc.). In this paper we are dealing with the macroscopic form of discontinuity. For nerve axons the effects of changes in radius have been extensively studied, particularly in reference to spinal motoneuron axon to soma propagation or the effects of axonal branch points (Goldstein and Rall, 1974; Westerfield et al., 1978; Joyner et al., 1980). Although the same concepts of changes in the electrical load encountered by a propagating action potential are applied to explain effects seen at branching cardiac trabeculae (Cranefield, et al., 1971; Spach et al., 1982) or at the Purkinje-ventricular junction (Mendez et al., 1969), it is not obvious that a cardiac strand with a varying strand radius is affected in the same way as a nerve axon with a varying cell radius. We have derived comparable expressions for passive cable properties of axons and strands and simulated action potential propagation along axons and strands of comparable anatomical variations. The results show that propagation in strands of cells is actually somewhat more sensitive to regional anatomical variations than is propagation in axons.

Another major difference between axons and strands is that the cytoplasmic resistivity of the axon is generally assumed to represent a continuous medium, while the longitudinal resistivity of a cardiac strand is clearly composed of a series combination of cytoplasmic resistivity and intercellular resistivity and, in addition, has been shown to be quite variable in different regions of the heart and also to be increased (or decreased) by a variety of interventions (see reviews by deMello, 1982; Wojtczak, 1982). We have studied the effects of a localized increase in longitudinal resistivity (comparable with a localized decrease in the number of intercellular gap junctions) and shown that unidirectional block of propagation may occur if this resistive barrier separates regions that are intrinsically different either in excitability or in membrane surface area. However, under some conditions in which the resistive barrier separates regions of differing electrical load, the resistive barrier may actually facilitate propagation between the two regions.

METHODS

A cardiac strand is composed of many individual cells, with irregular shapes, as shown in Fig. 1. We assume the cells have a constant

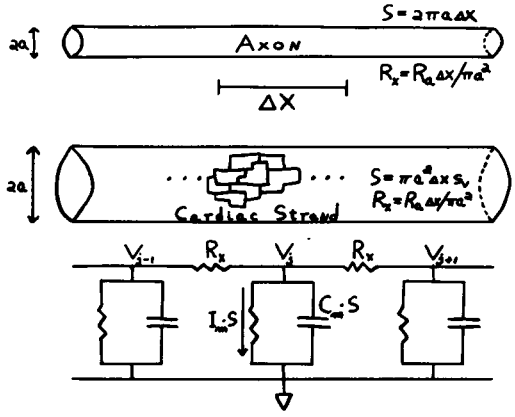

FIGURE 1 Diagram of an axon (*top*) a cardiac strand (*middle*) and an equivalent cable network that can represent the electrical properties of either the axon or the strand with the appropriate definitions of S (the surface area of a length Δx) and R_x (the resistance, Ω) between the centers of two adjacent segments (see text).

surface-to-volume ratio, S_v, and are electrically coupled such that the combination of cytoplasmic and intercellular resistance produces a net longitudinal resistivity R_a (Ωcm). For any cross section of the strand, the number of cells intersected will be proportional to a^2, where a is the strand radius. For a short length, Δx, of the strand we will assume that the cells are isopotential and have a total membrane area of $\pi a^2 \Delta x S_v$ (volume × surface/volume), or NS_vV_c, where V_c is the average cell volume and N is the number of cells contained within the volume $\pi a^2 \Delta x$. Thus, $N = \pi a^2 \Delta x / V_c$. From the equivalent circuit shown in the figure, we can derive, for a homogeneous strand (see Joyner et al., 1982)

$$\frac{1}{R_a S_v} \frac{V_{j-1} - 2V_j + V_{j+1}}{\Delta x^2} = C_m \frac{\partial V_j}{\partial t} + I_m. \quad (1)$$

We introduce a superscript to indicate time, with V_j^t being the membrane potential of segment j at time t. We approximate $\partial V/\partial t$ as a forward difference, $(V_j^{t+\Delta t} - V_j^t)/\Delta t$. We replace the second central difference (see Crank and Nicholson, 1947) with the average of the second central difference at time t and at time $t + \Delta t$. We can then rearrange to

$$-KV_{j-1}^{t+\Delta t} + (2K + 1)V_j^{t+\Delta t} - KV_{j+1}^{t+\Delta t} = K(V_{j-1}^t + V_{j+1}^t) - 2(K - 1)V_j^t - \Delta t I_m / C_m, \quad (2)$$

where $K = \Delta t/(2\, R_a C_m S_v \Delta x^2)$ for each segment j. This has the general form of

$$b_j V_{j-1}^{t+\Delta t} + d_j V_j^{t+\Delta t} + a_j V_{j+1}^{t+\Delta t} = c_j \quad (3)$$

As described previously (see Lieberman et al., 1973; Joyner et al., 1980) this set of equations can be easily solved at each time step for $V_j^{t+\Delta t}$ for $j = 1, 2, \ldots M$ by matrix techniques because the right-hand terms are known.

If we now allow the strand to be spatially inhomogeneous, we must describe the parameters S (the surface area of each segment) and R_x (the resistance in ohms between the centers of two adjacent segments) as functions of distance along the strand. We define $a(x)$, $I_m(x)$, $R_a(x)$, $N(x)$, and $S_v(x)$; then derive S(x) and $R_x(x)$. Note that $R_x(x)$ will be derived as the resistance for a length Δx to the right along the strand from location x. In discrete terms, if x is defined as zero at the left end of the strand, then each of these parameters is assumed constant over each discrete segment length so the actual form used in the simulation is, for each parameter, a set of values (e.g., $S_v[1]$, for each parameter, a set of values (e.g., $S_v[1]$, $S_v[2]$, ... $S_v[M]$) corresponding to the M segments used for the simulation. With these conventions

$$S(j) = \pi a^2(j) \Delta x S_v(j) \quad (4a)$$

$$R_x(j) = \frac{R_a(j)x}{2\pi a^2(j)} + \frac{R_a(j+1)x}{2\pi a^2(j+1)}. \quad (4b)$$

The basic equation derived from the conservation of current at segment j is now

$$\frac{V_{j-1} - V_j}{R_x(j-1)} - \frac{V_j - V_{j+1}}{R_x(j)} = S(j)[C_m \partial V/\partial t + I_m(j)]. \quad (5)$$

As in the Crank-Nicholson method, we substitute the average of V values at time t and time $t + \Delta t$ for the terms on the left and rearrange as

$$-K'(j)V_{j-1}^{t+\Delta t} + [K(j) + K'(j) + 1]V_j^{t+\Delta t} - KV_{j+1}^{t+\Delta t} = K'(j)V_{j-1}^t + K(j)V_{j+1}^t - [K'(j) + K(j) - 1]V_j^t - \Delta t I_m / C_m, \quad (6)$$

where $K(j) = \Delta t/2S(j)C_mR_x(j)$ and $K'(j) = \Delta t/2S(j)C_MR_x(j-1)$. This equation has the same general form as Eq. 3 except now $b_j = -K'(j)$, $a_j = -K(j)$, $d_j = K'(j) + K'(j) + 1$, and c_j equals the right side of Eq. 6 and the solution method is identical.

One important aspect of this general numerical technique is that the definition of $S_v(j)$ becomes the only difference in the method for axons or strands. Specifically, for an axon $S_v(j) = 2/a(j)$, while for a strand of electrically coupled cells $a(j)$ and $S_v(j)$ are separately defined as the strand radius and the cell surface-to-volume ratio, respectively.

If the I_m function is simply resistive (i.e., $I_m = V_j/R_m$), where R_m is the specific membrane resistivity (Ωcm²), then Eq. 1 can be written, for a spatially homogeneous strand or axon as

$$L^2 \frac{\partial^2 V}{\partial x^2} = T \frac{\partial V}{\partial t} + V, \quad (7)$$

where L is the length constant and T is the time constant. $L^2 = aR_m/2R_a$ for the axon and $L^2 = R_m/R_aS_v$ for the strand, independent of the strand radius. The time constant, T, is R_mC_m for both. The input resistance for current injected into the center of an axon or strand of infinite length is $(r_m r_a)^{1/2}$, where r_m is the membrane resistance per unit length (Ωcm) and r_a is the longitudinal resistance per unit length (Ω/cm). For the axon, $r_m = R_m/2\pi a$ and $r_a = R_a/\pi a^2$. For the strand, $r_m = R_m/\pi a^2 S_v$ and $r_a = R_a/\pi a^2$. The input resistance for the axon is $(R_mR_a/\pi^2a^3)^{1/2}$ and for the strand is $(R_mR_a/\pi^2a^4S_v)^{1/2}$. Notice that the dependence of the input resistance on the radius is different for the axon vs. the strand. For the strand the parameter a is the strand radius and the input resistance varies with a^{-2}. For the axon the parameter a is the cell radius and the input resistance varies with $a^{-1.5}$.

Simulations were programmed in FORTRAN on a VAX 11/780 digital computer (Digital Equipment Corp., Marlboro, MA). In the initial phase of the program the strand (or axon) parameters are set up, with computation of $S(j)$, $R_x(j)$, $K(j)$, $K'(j)$, b_j, a_j, and d_j. At each time step, the function $I_m(j)$ is evaluated for each segment and then used to compute the array c_j. The matrix equation formed by Eq. 6 is then solved for $V_j^{t+\Delta t}$ for $j = 1, 2, \ldots M$. The specific I_m functions are (*a*) the ventricular (V) model of Beeler and Reuter (1977) and (*b*) the Purkinje (P) model of McAllister et al. (1975). In the comparisons of propagation in strands with axons, we use the V model for both the strand and the axon to emphasize the differences produced by the cable description rather than differences in membrane properties. We used a segment length, Δx, of 50 μm as a discrete approximation of the syncytial structure. For the membrane models and the values of S_v and R_a used, the resting length constant is ~1 mm. We evaluated in a previous publication (Joyner, 1982) the effects of the discrete segment length on conduction velocity and maximum rate of rise, finding that, for $\Delta x = 50$ μm, both parameters were within 1% of the values obtained for $\Delta x = 10$ μm.

RESULTS

Surface-to-Volume Ratio as a Scaling Factor

For homogeneous action potential propagation, S_v can be considered as a scaling factor for propagation velocity in a strand in the same sense that the radius acts as a scaling factor for propagation in an axon. By using the substitution $\partial^2V/\partial t^2 = \theta^2\partial^2V/\partial x^2$, Eq. 1 can be written as follows for the special case of uniform propagation

$$\frac{d^2V}{dt^2} = A\frac{dV}{dt} + B,$$

where $B = R_a\theta^2S_vI_m$ and $A = 2R_a\theta^2C_m/a$ for the axon or $A = R_aS_v\theta^2C_m$ for the strand. The action potential shape, $V(t)$, and the conduction velocity, θ, are completely determined by the constants A and B. For a given I_m and C_m, θ^2 must vary directly with the axon radius, a, and inversely with R_a. For the strand, θ^2 must vary inversely with S_v and with R_a. In addition, any combination of R_a, S_v, C_m, I_m, and a that produce the same parameters A and B must also produce the same action potential shape and conduction velocity (see Hodgkin, 1954).

Effects of Radius Changes: Strand vs. Axon

Assume that the radius of the strand (or axon) is increased over a discrete region from a value a to a value a'. We can simulate action potential propagation for either the strand or the axon under conditions in which the membrane properties are identical and the propagation parameters are identical in the region where radius equals a. We use the membrane model of Beeler and Reuter (1977) and a value for S_v of 5,000 cm^{-1} (Sommer and Johnson, 1979). For the axon, the corresponding radius is $2/S_v = 0.0004$ cm. Fig. 2 shows the resulting distribution of $\dot{V}_{max}$ and

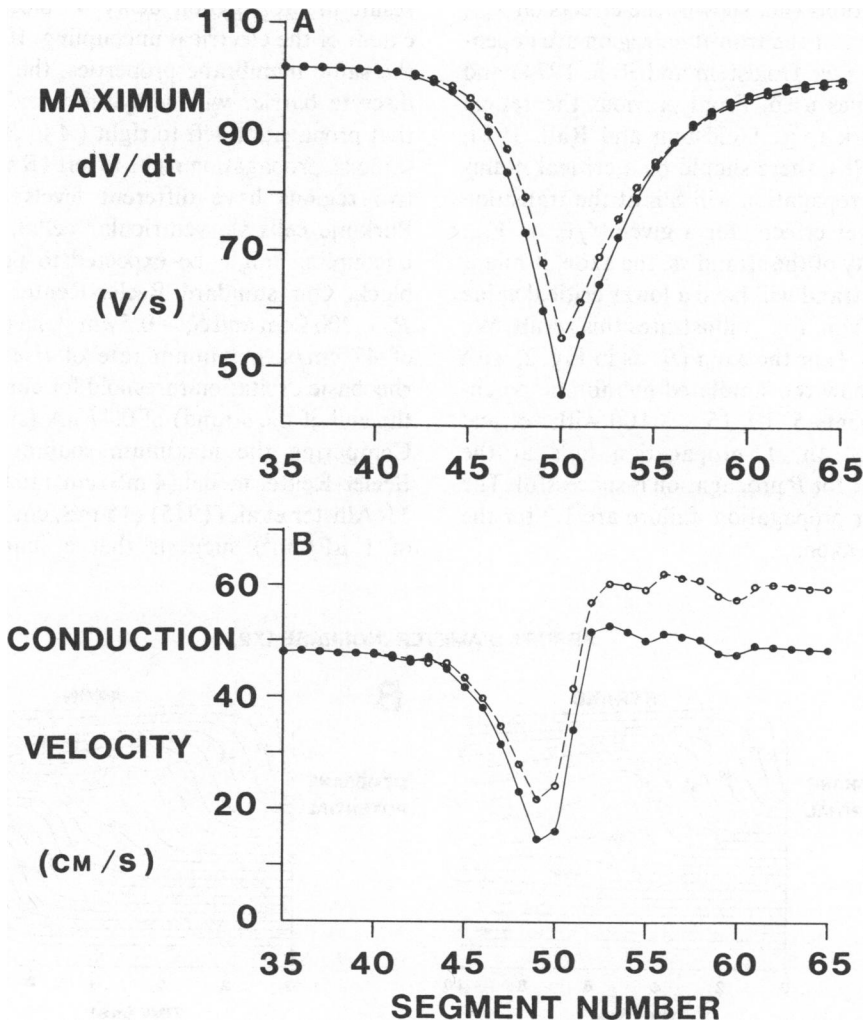

FIGURE 2 Effects of an abrupt increase in the radius of an axon or a cardiac strand. The spatial distribution of $\dot{V}_{max}$ (A) and conduction velocity (B) are plotted for simulations of a cardiac strand (○, dashed lines) or the axon (●, solid lines). For both the axon and the strand the radius was increased by 50% for segments 51–100. For the strand, all segments had $S_v = 0.5$ μm^{-1}. Propagation is from left to right. For the axon the radius of segments was 4 μm. Segment length 50 μm, R_a 200 Ωcm. Beeler-Reuter membrane model.

conduction velocity along the axis of the strand (open circles) or axon (filled circles) when the strand or axon radius is increased by 50% for segments 51–100 (propagation is from left to right, stimulating segment 1). Note several features. (*a*) For the axon, the conduction velocity is proportional to $a^{1/2}$, with an increased conduction velocity in the region of increased radius. For the strand, the conduction velocity is independent of the strand radius except at the transition region. However, it must be understood that the shape of the action potential is changing at the transition region, so a precise definition of conduction velocity at this region is not possible. We have defined the arrival time of the action potential at each segment as the time at which that segment has its peak inward current. (*b*) The axon and the strand are similarly affected at the transition region, in terms of the changes in $\dot{V}_{max}$ and conduction velocity, but the changes in both $\dot{V}_{max}$ and conduction velocity are larger for the strand than for the axon.

From other simulations (not shown) the effects on $\dot{V}_{max}$ and conduction velocity at the transition region are dependent on the ratio a'/a (see Goldstein and Rall, 1974) and not on the actual values used. From previous theoretical and experimental work (e.g., Goldstein and Rall, 1974; Westerfield et al., 1978), there should be a critical radius ratio a'/a for which propagation will fail at the transition region. From the larger effects, for a given a'/a, on $\dot{V}_{max}$ and conduction velocity of the strand vs. the axon, it might be expected that the strand will have a lower critical value of a'/a than will the axon. Fig. 3 illustrates this result. We simulated the strand (*A*) or the axon (*B*) as in Fig. 2, with $a'/a = 2$. The plots show the simulated membrane potential vs. time for segments 5, 10, 15, ... 100 with vertical separation for clarity. In *A*, propagation fails at the transition region, while for *B* propagation is successful. The critical a'/a values for propagation failure are 1.9 for the strand and 2.4 for the axon.

Effects of a Resistive Barrier

Regions of increased cell-cell resistance can exist either by a uniformly distributed decrease in the number of gap junctions or the interposition of connective tissue between layers of conducting cells. Specific examples include the atrio-ventricular node, uncoupling in ischemic areas, and the separation of endocardial Purkinje fibers from the underlying myocardium (see deMello, 1982). In all of these situations, there is a functional increase in the intercellular resistance in the direction of propagation, which can be represented in a one-dimensional sense by a spatial distribution of $R_a(j)$. In the simplest case, consider a strand with two regions, *A* and *B*. Within either region the coupling resistance is normal (in our model, 200 Ωcm), but at the junctional region there is a discrete region of high coupling resistance. A propagating action potential in region *A* must cross the resistive barrier to activate region *B*. As previously shown (Joyner, 1982) such a barrier will result in propagation delay or block, depending on the extent of the electrical uncoupling. If the two regions have the same membrane properties, the block produced by a discrete barrier will be symmetrical if present, meaning that propagation left to right (*A* to *B*) will be affected the same as propagation right to left (*B* to *A*). However, if the two regions have different levels of excitability (e.g., Purkinje cells vs. ventricular cells), a discrete region of uncoupling might be expected to produce unidirectional block. Our standard Beeler-Reuter (1977) model, with $R_a = 200$ Ωcm and $S_v = 0.5$ μm^{-1}, has a conduction velocity of 47 cm/s, maximum rate of rise of 105 V/s, and an rheobasic excitation threshold for current (I_{th}, injected into the end of the strand) of 0.47 μA (strand radius 100 μm). Comparing the maximum sodium conductance of the Beeler-Reuter model (4 mS/cm^2) to that of the P model of McAllister et al. (1975) (15 mS/cm^2 when scaled for a C_m of 1 μF/cm^2) suggests that a fourfold increase in the

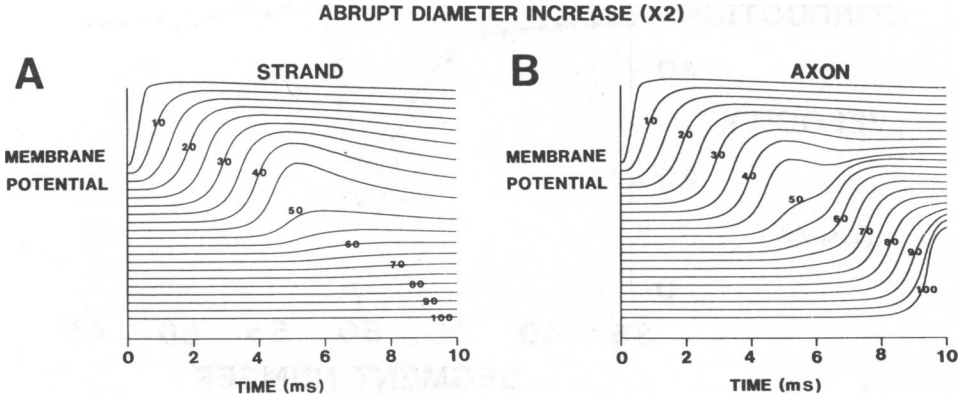

FIGURE 3 Plots of voltage vs. time for selected segments (5, 10, 15 ... 100) of a simulated cardiac strand (*A*) and an axon (*B*) in which the radius was increased by 100% for segments 51–100. For the strand all segments had $S_v = 0.5$ μm^{-1}. Segment length 50 μm. R_a 200 Ωcm. Beeler-Reuter membrane model.

maximum sodium conductance might be appropriate to model the excitability difference between the two types of tissues. Table I shows the effects of changing the maximum sodium conductance in the Beeler-Reuter model, over a tenfold range, on conduction velocity, $\dot{V}_{max}$, and I_{th}.

Fig. 4 shows how the maximum conductance affects $\dot{V}_{max}$, conduction velocity, and I_{th} with the results expressed in terms of values normalized to the values obtained with the standard value of 4 mS/cm^2 for sodium conductance. With the normalized values and the sodium conductance both plotted logarithmically, the slopes of the relationships show the sensitivity of each parameter as a power function. Thus, $\dot{V}_{max}$, conduction velocity and I_{th} approximately vary with g_{Na}^{y}, where y equals 0.93, 0.37, and 0.24, respectively, for the particular membrane model used in these simulations (Beeler and Reuter, 1977).

Having shown, as expected, that increases in the sodium conductance increase the excitability of the strand, we would anticipate that increases in sodium conductance would allow propagation to occur across a resistive barrier that would otherwise produce propagation failure. Fig. 5 shows the results of simulations of strands with 100 segments with the normal value of R_a = 200 Ωcm for all segments except segment 50, where we used a higher value of R_a and found the critical value of this localized increase in longitudinal resistivity for propagation failure. Stimulation was done at the left end (segment 1) and the critical resistance was evaluated for three distributions of sodium conductance. (*1*) The increased sodium conductance, as plotted on the abscissa, was used for all 100 segments of the strand (filled circles), (*2*) segments 1–50 retained the standard sodium conductance, while segments 51–100 had the increased sodium conductance (open circles), and (*3*) segments 1–50 had the increased sodium conductance, while segments 51–100 retained the standard sodium conductance (open triangles). The ordinate is plotted logarithmically as the critical resistivity normalized to the value obtained for the strand with all segments having the standard sodium conductance. Increasing sodium conductance increases, as expected, the critical localized resistivity for propagation failure of the homogeneous strand (filled circles). For the asymmetrical strand(regions *A* and

TABLE I
EFFECTS OF INCREASING SODIUM CONDUCTANCE ON PROPAGATION PARAMETERS

$\bar{G}_{Na}$	Velocity	$\dot{V}_{max}$	I_{th}
mS²/cm	*cm/s*	*V/s*	*μA*
4	47 (1)	105 (1)	0.47 (1)
8	66 (1.40)	237 (2.26)	0.40 (0.85)
16	85 (1.81)	448 (4.27)	0.34 (0.73)
40	110 (2.34)	898 (8.55)	0.27 (0.57)

Numbers in parentheses are ratios with respect to the normal values for $\bar{G}_{Na}$ = 4 mS/cm^2.

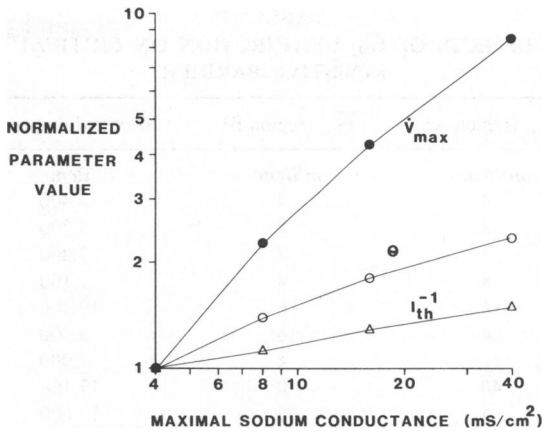

FIGURE 4 Changes in $\bar{G}_{Na}$ have different effects on various propagation parameters. We used homogeneous strand simulations with variable $\bar{G}_{Na}$ to obtain the relationship of $\dot{V}_{max}$, conduction velocity, and I_{th}^{-} to $\bar{G}_{Na}$, with results normalized to the values obtained for $\bar{G}_{Na}$ = 4 mS/cm^2.

B having different values for sodium conductance), there is an asymmetrical effect of a resistive barrier. For propagation from a region of lower excitability to a region of higher excitability (open circles), a higher value of junctional resistivity can be tolerated than for propagation from a region of higher excitability to a region of lower excitability (open triangles). This effect clearly presents the possibility of unidirectional block of propagation across a resistive barrier separating regions with different levels of excitability. Table II shows the values of critical resistivity that

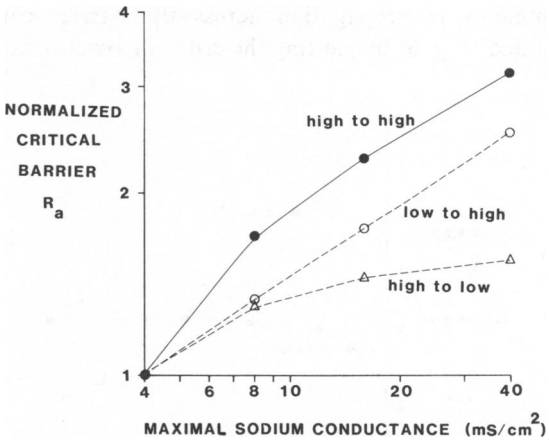

FIGURE 5 A resistive barrier produces asymmetrical effects if the proximal and distal regions have different levels of excitability. We used simulations of 100-segment cables in which the critically high resistivity between segments 50 and 51 was obtained under three different distributions of excitability. Results are normalized to the values obtained for all segments having $\bar{G}_{Na}$ = 4 mS/cm^2. Results are shown for (*a*) both proximal and distal regions have increased $\bar{G}_{Na}$ as indicated on the abscissa (●), (*b*) only the distal region had the increased $\bar{G}_{Na}$ (○), and (*c*) only the proximal region had the increased $\bar{G}_{Na}$ (△). Segment length 50 μm, R_a 200 Ωcm except at the barrier, Beeler-Reuter membrane model with $\bar{G}_{Na}$ adjusted as noted.

TABLE II
EFFECTS OF $\bar{G}_{Na}$ DISTRIBUTION ON CRITICAL RESISTIVE BARRIER

$\bar{G}_{Na}$ (region A)	$\bar{G}_{Na}$ (region B)	Maximal resistivity
mS/cm²	*mS/cm²*	*Ωcm*
4	4	5,400
8	8	9,200
4	8	7,250
8	4	7,100
16	16	12,300
4	16	9,200
16	4	7,900
40	40	17,100
4	40	13,600
40	4	8,400

produced block of propagation with the Beeler-Reuter model with variable sodium conductance and a segment length of 50 μm.

Two regions separated by a resistive barrier may differ in ways other than simply a difference in excitability. In a multidimensional system, a small region may be partially insulated from a much larger volume of surrounding tissue. In addition, the cells within the two regions could have different shapes and sizes, producing a regional difference in S_v and, therefore, a regional difference in the resting length constant. We can illustrate these effects by using a one-dimensional strand in which the resistive barrier is asymmetrically located, making region *A* shorter than region *B*. We will use enough segments in the model such that region *B* can be considered to be infinitely long. Asymmetry in propagation across the barrier can be evaluated (Fig. 6) by plotting the critical barrier resistivity as a function of the length of region *A* for propagation from *A* to *B* (filled circles) and from *B* to *A* (open circles). As region *A* becomes shorter, the input resistance of region *A* increases and the input capacitance decreases, reducing the amount of current required to flow across the barrier from *B* to *A* to excite region *A*. This effect allows the critical barrier resistivity to be increased for propagation from *B* to *A*. However, the smaller area of region *A* is less capable of generating current across the barrier into the constant electrical load of region *B*, so the critical barrier resistivity for propagation *A* to *B* is decreased as the length of region *A* is decreased. As in the case of two regions with different levels of excitability, two regions with differences in membrane area may show unidirectional block of propagation across a resistive barrier.

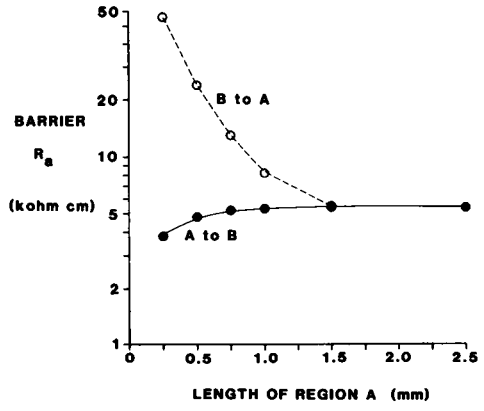

FIGURE 6 A resistive barrier produces asymmetrical effects if the proximal and distal regions have different values of electrical load. We used a 100-segment cable simulation with the resistive barrier placed such that region *A* (to the left of the barrier) was shorter than region *B* (to the right of the barrier). For each barrier location we plot, as a function of the length of region *A*, the critical barrier resistivity for propagation failure when we stimulated segment 1 (*A* to *B*, ●) or segment 100 (*B* to *A*, ○). Segment length 50 μm, R_a 200 Ωcm except at the barrier, Beeler-Reuter membrane model.

A Resistive Barrier Can Facilitate Propagation Through a Region of Increasing Electrical Load

Cardiac anatomy presents a variety of normal regions in which the propagating action potential encounters an increasing electrical load. One obvious example is that any region of action potential initiation (e.g., the sinoatrial node) must cope with the large electrical load of the surrounding nonpacing tissue. Another example is the junctional region between the small diameter Purkinje strand and the large papillary muscle (Mendez et al., 1969). Mendez et al. discuss this phenomenon as an anatomical funnel leading to a low safety factor and a delay in propagation from Purkinje (P) to ventricular (V) cells. The P strand diameter remains nearly constant as it approaches the muscle surface, providing a short length over which the funneling of the effective diameter must occur. Our recent experimental work (Veenstra et al., 1984) indicates that the diameter of the region of the papillary muscle directly activated by the P strand is on the order of four times the diameter of the P strand. Thus, in a one-dimensional sense, the P-V junction can be considered as a strand in which region *A* has a constant small radius except near the beginning of the *B* region of larger diameter. Over a relatively short distance at the junctional region of the strand, the radius funnels from the smaller value to the larger value. In our simulation we use a 100-segment cable in which the segment length is 50 μm. The radius of segments 1–44 is 1.5 mm, while the radius of segments 51–100 is 6.0 mm. The radii of segments 45–50 are calculated to give a funnel length of ~300 μm (6 segments). Segments 1–50 have the P membrane model (I_m function from McAllister et al., 1975), while segments 51–100 have the V membrane model (I_m function from Beeler and Reuter, 1977). Fig. 7 *A* shows the simulated action potential propagation for this strand. The action potential propagates through the initial region corresponding to the P strand, but fails to propagate through the junctional region into the ventricular region (segments

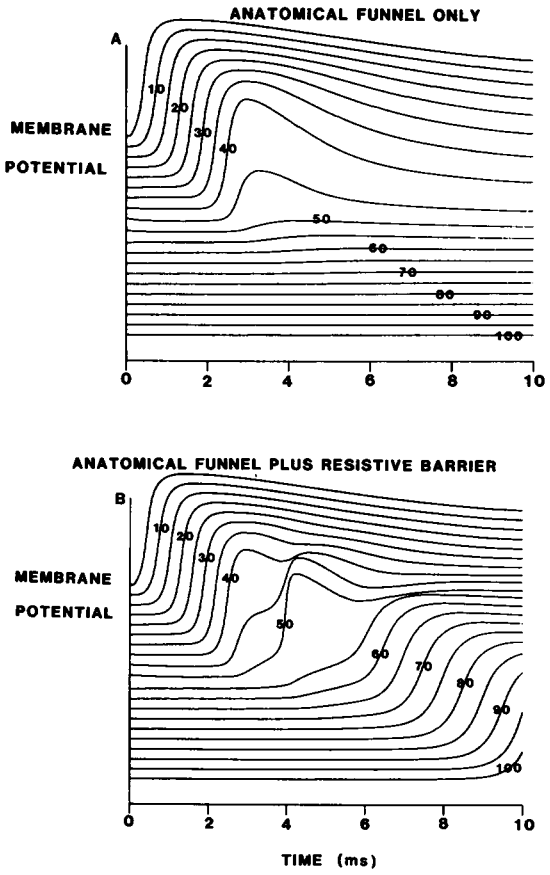

FIGURE 7 A resistive barrier can sometimes facilitate propagation. We simulated a Purkinje strand attached to a larger ventricular strand by a cable with 100 segments in which segments 51–100 had a radius of 6 mm, segments 1–44 had a radius of 1.5 mm, and segments 44–50 had a progressive increase in radius from 1.5 to 6 mm. For *A* and *B* we plot the simulated membrane potential as a function of time for segments 5, 10, 15 . . . 100 with a resistive barrier of 3,000 Ωcm placed between segments 50 and 51 for the simulation of *B*. Segments 1–50 had the P membrane model. Segments 51–100 had the V membrane model. Segment length 50 μm.

51–100). The cause of the propagation failure is the nearly abrupt increase in radius, producing an increase in electrical load. If we now include in our model a relative lack of cell-cell coupling between the P cells and the V cells, as demonstrated anatomically by Martinez-Palomo et al. (1970), we get the result shown in Fig. 7 *B*. The only change in the model between parts *A* and *B* is that we have used, for *B*, a localized resistive barrier of 3,000 Ωcm (over 50 μm) between segments 50 and 51. Propagation is now successful across the junctional region. From this and other simulations (not shown) we have found that, for a given anatomical funnel producing action potential propagation failure by an increased electrical load, there is a range of values for the resistivity of the barrier for which propagation will be successful. For values less than this range, propagation failure occurs because the electrical load increase is still sufficient to block propagation. For values greater than this range, propagation failure occurs because the resistive barrier does not allow enough current to enter the distal region to produce excitation. For the particular geometry used for Fig. 7, propagation was successful when the localized resistive barrier was >800 Ωcm and <3,950 Ωcm over the 50-μm segment length.

DISCUSSION

We have introduced a modification of the core conductor model for action potential propagation (Lieberman et al., 1973; Sharp and Joyner, 1980) that now explicitly includes the surface-to-volume ratio of the cells and the radius of the cardiac strand as independent parameters. In one sense, this represents another scaling factor for conduction velocity (similar to R_a) because changes in S_v do not change action potential shape as a function of time at any given location. However, this modification is significant in that we can now clearly show the consequences of the normal inhomogeneous macroscopic anatomy of cell bundles (trabeculae) fusing and dividing in an irregular fashion. For axons, $S_v = 2/a$, where a is the cell radius. Thus, conduction velocity and length constant depend on the axon radius, as is well known. However, for a cardiac strand, conduction velocity and length constant are independent of the strand radius but do depend of the S_v of the individual cells. The consequences of regional changes in strand radius are similar to but quantitatively different from the consequences of regional changes in an axon radius. In both cases an increased radius presents an increased electrical load on a propagating action potential, but the effect is more marked for a strand than for an axon (Fig. 2).

The transient decrease in conduction velocity and $\dot{V}_{max}$ at a region of increased radius is associated with a lowered safety factor, with conduction failure at a critical value of the ratio of the two radii (Goldstein and Rall, 1974; Westerfield et al., 1978). For any given membrane model the critical radius ratio for a strand is less than for an axon (Fig. 3). The large effects of the macroscopic anatomy on action potential propagation have recently been reviewed (Spach et al., 1982) with particular reference to branching trabeculae in the dog atrium.

It is clear from many studies (see deMello, 1982, for review) that the coupling resistance between cells is spatially inhomogeneous throughout the heart. Recent experimental work has shown that cell-cell coupling, in addition to being spatially inhomogeneous, may also be altered under conditions of altered internal pH or calcium concentration (Wojtczak, 1982). It has also been shown that there are directional differences in the coupling resistance (Clerc, 1976), and there is some evidence that the discrete size of the cell bundles produces effects that can be attributed to a discontinuous distribution of cell-cell coupling resistance (Spach et al., 1981; Joyner, 1982). Earlier studies on models of slow conduction (Lieberman et al., 1973) stressed spatially homogeneous uncoupling of cells

as a primary determinant of slow conduction in regions such as the atrio-ventricular node. In our previous work (Sharp and Joyner, 1980) we simulated propagation delay or block in a strand with a localized region of increased R_a, and have also shown (Joyner, 1981) that a spatially asymmetrical distribution of R_a could produce unidirectional block of action potential propagation.

When a simple resistive barrier, defined as a localized increase in the cell-cell coupling resistance is included in a strand that is also inhomogeneous with respect to strand radius and/or excitability, the resulting effects on propagation can either increase or decrease the safety factor for propagation. This change in safety factor can also be different for different directions of propagation, leading to the possibility of unidirectional block produced by a localized resistive barrier. As a simple way of altering excitability, we varied the maximal sodium conductance in the Beeler-Reuter (1977) model from the standard value of 4 mS/cm^2 up to 40 mS/cm^2. For a homogeneous strand, Fig. 4 shows the dependence of $\dot{V}_{max}$, conduction velocity and I_{th} on the maximal sodium conductance, with a decreasing sensitivity of these three parameters, respectively, on $\overline{G}_{Na}$. $\dot{V}_{max}$ is most sensitive to changes in $\overline{G}_{Na}$ because $\dot{V}_{max}$ occurs at a time when the membrane conductance is very high and is thus relatively independent of the passive cable properties of the strand. I_{th} is relatively insensitive to $\overline{G}_{Na}$ because I_{th} is primarily determined by the passive cable properties and is altered by changes in $\overline{G}_{Na}$ only by the extent to which the threshold voltage is lowered. Conduction velocity depends on $\overline{G}_{Na}$ with an intermediate sensitivity because of the more nearly equal contribution of membrane excitability and cable properties to this parameter.

In discussing the effects of the resistive barrier, it is helpful to clarify the concept of safety factor for propagation. As we discussed previously (Joyner, 1982) the safety factor for propagation can be defined at a particular location, and for a particular direction of propagation, as the ratio of the current that can be supplied by the proximal cells to the current required to bring the distal cells to a voltage level sufficient to initite a propagating action potential. Across a barrier of any type, the current that the proximal region can supply is increased by increasing the action potential amplitude or decreasing the resistance of the barrier. Increases in $\overline{G}_{Na}$ proximal to the barrier increase the action potential amplitude proximal to the barrier and thus the amount of current that can be supplied. The current required to excite the distal region (through the barrier) is independent of the barrier resistance but is dependent on the cable properties and the excitability of the distal region. Increases in $\overline{G}_{Na}$ distal to the barrier decrease the amount of current required to initiate a propagating action potential.

As shown in Fig. 5, the maximum resistivity of a barrier separating two parts of a cardiac strand is increased by increasing the excitability on the proximal and/or distal region. The effect becomes asymmetrical when the excitability difference is large, with propagation favored in the direction of low to high excitability. When a resistive barrier connects two regions of different electrical load, the asymmetry in maximal barrier resistivity for successful propagation is even more apparent (Fig. 6). For a small region, the input impedance is very high during the charging phase before action potential initiation, allowing an adequate amount of charging current to flow across a very high barrier resistance (propagation *B* to *A*, open circles). However, if the action potential is directly initiated in the small region, the effective length of this small region becomes longer due to a decreased membrane resistance and thus its ability to send current through the barrier to excite the larger region is only slightly diminished (propagation *A* to *B*, filled circles).

We applied our simulation technique to the specific example of the Purkinje-ventricular junction (PVJ), with a somewhat paradoxical result of a facilitation of propagation by a resistive barrier. The known anatomy and excitability differences are modeled as a anatomical funnel (cf., Mendez et al., 1969) with higher excitability (MNT model) for the Purkinje cells than for the ventricular cells (BR model). We emphasize that our PVJ model is very approximate. The membrane models we used have quantitative limitations, but do approximate the known differences in $\dot{V}_{max}$ (300 V/s for P, 100 V/s for V). The actual anatomy is quite variable but the P strands are always small in comparison with the papillary muscle. While more experimental data are required to make a realistic anatomical model, the principle illustrated in Fig. 7 can be simply explained. When we simulate the PVJ with homogeneous resistivity (Fig. 7 *A*) propagation fails at the junctional region due to the large electrical load of the V region. Our model actually underestimates the load of the V region because we used a radius of the V region equal to the amount of V cells directly activated by the P cells and did not include the multidimensional nature of the papillary muscle. The MNT model underestimates the $\dot{V}_{max}$ of the P cells by perhaps a factor of 2. However, Fig. 5 shows that if the ratio of $\overline{G}_{Na}$ in the proximal region to $\overline{G}_{Na}$ in the distal region is already as high as 4, further increases in the proximal $\overline{G}_{Na}$ do not have much effect on the safety factor for propagation. The length of 300 μm chosen for the funnel comes from observations of the thickness of the layer of P cells on the papillary muscle near the site of anatomical junction of the P strand and the papillary muscle. The facilitation of propagation produced by the presence of the resistive barrier (Fig. 7 *B*) can be explained on the basis of increasing the amount of current that can be supplied from the P cells to the V cells. Even though the coupling resistance between the P cells and the V cells is now higher, this is more than offset by the increased amplitude of the P cell action potential just proximal to the barrier (compare segment 50 in *A* and *B* of Fig. 7).

Our recent studies (Veenstra et al., 1984) have produced some electrophysiological data that suggest that the

endocardial ventricular cells are separated by a resistive barrier from a superficial layer of Purkinje cells. We studied in vitro dog papillary muscles with both intracellular and extracellular electrodes to produce activation maps of the P and V cell layers. We found that the action potential duration (APD) of the P layer decreased as the action potential propagated from free-running strands into the superficial layer, but there remained a discrete difference of 50–70 ms between P APD and V APD even at sites where, from the mapping studies, it was clear that the action potential was propagating from the P layer into the V layer. The data indicate that the resistive barrier is inhomogeneously distributed with large regions having bidirectional block of propagation between the P and V layers, presumably due to a high resistive barrier. We found that all regions at which propagation could occur from P to V would also allow propagation from V to P. However, some regions would allow propagation V to P but not propagation P to V, illustrating a form of potential unidirectional block. Two factors demonstrated here may be responsible for this phenomenon. The P layer, as compared with the V layer, has a higher excitability and a lower thickness. Thus, the asymmetry of propagation across a resistive barrier illustrated in Fig. 5 (favoring propagation from low to high excitability) and in Fig. 6 (favoring propagation from a large area to a small area) may both contribute to the demonstrated unidirectional block.

We propose that the normal presence of a resistive barrier between P cells and V cells produces at least a partial dissociation between the two cell layers. This allows the P layer to propagate rapidly around the endocardium to synchronize the ventricular activation. The resistive barrier may actually facilitate ventricular activation, while maintaining a P layer APD that is longer than the V layer APD. This longer P layer APD may serve to block the propagation into the P layer of early ventricular premature beats (Myerburg et al., 1971). However, under conditions of myocardial ischemia, the spatial distribution of the resistive barrier may be changed, due to the well documented deleterious effects of cell injury on gap junctions. Regional ischemia may convert regions of the endocardium into completely dissociated P and V layers. This would produce a greater probability of ectopic foci, since the P automaticity would no longer be suppressed by electrical coupling to the V layer and also may facilitate reentry due to the presence of regions of unidirectional block and slow ventricular conduction.

This work was supported by a National Institutes of Health grant HL22562 and Iowa Heart Association grant 82-G-26 to Dr. R. W. Joyner.

Received for publication 2 June 1983 and in final form 18 December 1983.

REFERENCES

Beeler, G. W., and H. Reuter. 1977. Reconstruction of the action potential of myocardial fibres. *J. Physiol. (Lond.).* 268:177–210.

Clerc, L. 1976. Directional differences of impulse spread in trabecular muscle from mammalian heart. *J. Physiol. (Lond.).* 255:335–346.

Cranefield, P. F., and B. F. Hoffman. 1971. Conduction of the cardiac impulse. II. Summation and inhibition. *Circ. Res.* 28:220–233.

Crank, J., and P. Nicholson. 1947. A practical method for numerical evaluation of solutions of partial differential equations of the heat-conducting type. *Proc. Cambridge Phil. Soc.* 43:50–67.

deMello, W. C. 1982. On the control of cell communication in heart. *In* Cardiac Rate and Rhythm. L. N. Bouman and H. J. Jongsma, editors. Martinus Nijhoff Publishers, The Hague, The Netherlands. 179–194.

Hodgkin, A. L. 1954. A note on conduction velocity. *J. Physiol. (Lond.).* 125:221–224.

Goldstein, S., and W. Rall. 1974. Changes of action potential shape and velocity for changing core conductor geometry. *Biophys. J.* 14:731–757.

Joyner, R. W. 1981. Mechanisms of unidirectional block in cardiac tissues. *Biophys. J.* 35:113–125.

Joyner, R. W. 1982. Effects of the discrete pattern of electrical coupling of propagation through an electrical syncytium. *Circ. Res.* 50:192–200.

Joyner, R. W., M. Westerfield, and J. W. Moore. 1980. Effects of cellular geometry on current flow during a propagated action potential. *Biophys. J.* 31:183–194.

Lieberman, M., J. M. Kootsey, E. A. Johnson, and T. Sawanobori. 1973. Slow conduction in cardiac muscle. A biophysical model. *Biophys. J.* 13:37–55.

Martinez-Palomo, A., J. Alanis, and D. Benitez. 1970. Transitional cardiac cells of the conduction system of the dog heart. *J. Cell Biol.* 47:1–17.

McAllister, R. E., D. Noble, and R. W. Tsien. 1975. Reconstruction of the electrical activity of cardiac Purkinje fibres. *J. Physiol. (Lond.).* 251:1–59.

Mendez, C., W. J. Mueller, J. Meredith, and G. K. Moe. 1969. Interaction of transmembrane potentials in canine Purkinje fibers and at Purkinje fiber-muscle junctions. *Circ. Res.* 24:361–373.

Myerburg, R. J., H. Gelband, and B. F. Hoffman. 1971. Functional characteristics of the gating mechanism in the canine A-V conducting system. *Circ. Res.* 28:136–145.

Sharp, G. H., and R. W. Joyner. 1980. Simulated propagation of cardiac action potentials. *Biophys. J.* 31:403–424.

Sommer, J. R., and E. A. Johnson. 1979. Ultrastructure of cardiac muscle. *Handb. Physiol. Sect. 2.* 1:113–186.

Spach, M. S., W. T. Miller III, P. C. Dolber, J. M. Kootsey, J. R. Sommer, and C. E. Mosher, Jr. 1982. The functional role of structural complexities in the propagation of depolarization in the atrium of the dog. *Circ. Res.* 50:175–191.

Spach, M. S., W. T. Miller III, D. B. Geselewitz, R. C. Barr, J. M. Kootsey, and E. A. Johnson. 1981. The discontinuous nature of propagation in normal canine cardiac muscle. Evidence for recurrent discontinuities of intacellular resistance that affect the membrane currents. *Circ. Res.* 48:39–54.

Veenstra, R. D., R. W. Joyner, and D. A. Rawling. 1984. Purkinje and ventricular activation sequences of canine papillary muscle. *Circ. Res.* In press.

Westerfield, R. M., R. W. Joyner, and J. W. Moore. 1978. Temperature-sensitive conduction failure at axon branch points. *J. Neurophysiol.* 41:1–8.

Wojtczak, J. 1982. Intercellular coupling between cardiac cells and its disturbances. *In* Cardiac Rate and Rhythm. L. N. Bouman and H. J. Jongsma, editors. Martinus Nijhoff Publishers, The Hague, The Netherlands. 283–296.